Isolation of a virus causing a chronic infection in the archaeal model organism *Haloferax volcanii* reveals antiviral activities of a provirus

Tomas Alarcón-Schumacher[a], Adit Naor[b,1], Uri Gophna[b], and Susanne Erdmann[a,2]

Viruses are important ecological, biogeochemical, and evolutionary drivers in every environment. Upon infection, they often cause the lysis of the host cell. However, some viruses exhibit alternative life cycles, such as chronic infections without cell lysis. The nature and the impact of chronic infections in prokaryotic host organisms remains largely unknown. Here, we characterize a novel haloarchaeal virus, Haloferax volcanii pleomorphic virus 1 (HFPV-1), which is currently the only virus infecting the model haloarchaeon *Haloferax volcanii* DS2, and demonstrate that HFPV-1 and *H. volcanii* are a great model system to study virus–host interactions in archaea. HFPV-1 is a pleomorphic virus that causes a chronic infection with continuous release of virus particles, but host and virus coexist without cell lysis or the appearance of resistant cells. Despite an only minor impact of the infection on host growth, we uncovered an extensive remodeling of the transcriptional program of the host (up to 1,049 differentially expressed genes). These changes are highlighted by a down-regulation of two endogenous provirus regions in the host genome, and we show that HFPV-1 infection is strongly influenced by a cross-talk between HFPV-1 and one of the proviruses mediated by a superinfection-like exclusion mechanism. Furthermore, HFPV-1 has a surprisingly wide host range among haloarchaea, and purified virus DNA can cause an infection after transformation into the host, making HFPV-1 a candidate for being developed into a genetic tool for a range of so far inaccessible haloarchaea.

archaea | virus | chronic infection | CRISPR

Prokaryotic viruses are the most abundant and genetically diverse biological entities, and they have the potential to modulate microbial abundances, community structure, and the evolutionary trajectory of their hosts (1–3). The impact of viruses on their particular host and within the microbial community is largely determined by their lifestyle. Traditionally, viruses have been mainly considered as killing machines that do not have their own metabolism; instead, they hijack the host metabolic machinery and redirect it toward virus production that subsequently leads to the lysis of the host cell. Some viruses can enter into a lysogenic state, in which they integrate their genome into the host chromosome, are replicated with the chromosome, and, subsequently, are inherited by the cell progeny without host cell lysis. Nevertheless, environmental changes can induce the excision of the provirus to enter into a lytic life cycle.

When using traditional methods for virus isolation, such as plaque assay, that are based on host cell lysis or severe growth delay, viruses that cause chronic infections are often overlooked. During a so-called "productive chronic infection," virus particles are consistently released without lysis of the host cell, typically, by budding through the host cell membrane and incorporating host lipids (4–7). Chronic infections are common among eukaryotic viruses. However, only a few chronic viruses have been described for prokaryotes (8, 9), and the majority of them infect archaea (10–14).

Archaea share cellular characteristics with both bacteria and eukaryotes while exhibiting some unique characteristics, and so do their viruses (15). Accordingly, archaea and bacteria share many physiological and morphological traits, and a large proportion of the lytic viruses infecting archaea isolated to date have the classic head-tailed morphology of bacteriophages (16, 17). Meanwhile, recent characterization of novel archaeal clades has tightened the phylogenetic relationships between archaea and eukaryotes, and revealed that several intracellular processes, such as intracellular trafficking and vesicle formation and export, are carried out by homologous groups of proteins in archaea and eukaryotes (18, 19). These processes are crucial for the success of nonlytic viral infections, and the isolation and characterization of novel archaeal viruses has shown that virion morphogenesis and egress mechanisms in archaea largely resemble the

Significance

Viruses use a wide range of strategies to take over host cells for virus replication. While nonlytic infections are common in eukaryotic systems, little is known about those in prokaryotes. We report a virus causing a persistent infection in the model organism *Haloferax volcanii*. The infection cycle is characterized by high viral titers and stability over multiple generations but low impact on cell viability. The virus has a major impact on cell behavior, mainly by down-regulating host genes in unprecedented quantities, while interacting with a provirus region in the host genome, revealing an undescribed superinfection exclusion mechanism. This unique virus has an unusually wide host range and the potential to be developed into a versatile genetic tool in archaea.

budding of enveloped viruses in eukaryotes (20–23). Therefore, the study of chronic virus in archaea has the potential to provide insights into the molecular evolution of virus–host interactions in eukaryotes.

Given the relatively small number of characterized chronic infections in prokaryotes, virus–host interaction in archaea and the impact on microbial community dynamics and evolution of this particular lifestyle remains largely unexplored. Moreover, recent studies indicate that chronic cycles are more widespread in nature than previously thought (6, 9). The development of a stable yet controllable chronic infection in archaea will, therefore, significantly advance our understanding of the molecular basis and ecological impact of chronic viruses.

In most environments, viruses outnumber their host by a factor of 10, which means that not only must viruses evolve to overcome host defense mechanisms but also, due to a limited number of host cells, there is the need to outcompete other related viruses. Cells harbor a wide spectrum of mobile genetic elements from viral and nonviral origins such as plasmids, transposons, casposons, or proviruses (24). Particularly, proviruses are commonly found in archaeal and bacterial genomes, and ∼60% of the genomes contain, at least, intact functional forms or, defective in varying degrees, virus-like sequences (25, 26). At some point in their evolution, some of these proviruses have been immobilized by their hosts, and, through selection, the cells sometimes conserve viral sequences encoding for advantageous traits (27). For example, viral genes encoding for superinfection exclusion mechanisms, whose aim is to block further infections by competing viruses (28), can result in the emergence of a new defense system against viral infection (29, 30). Superinfection exclusion has been largely studied for bacterial viruses, and the nature and molecular basis of these mechanisms comprise an extremely wide variety of targets, such as blocking the adsorption of viruses through modifications to the cell envelope, inhibiting the genome replication of a competing virus, or inhibiting the activity of lysozymes when lytic cycles are underway (30–32). However, the possibility of superinfection has, so far, only been observed for an isolated archaeal rod-shaped virus from the family *Rudiviridae*, although the mechanism remains unknown (33). Superinfection exclusion has also been proposed to occur in icosahedral, nonlytic viruses of the family *Portogloboviridae* through virus-encoded CRISPR arrays (34).

Here we characterize a virus causing a chronic productive life cycle, isolated for the model organisms *Haloferax volcanii* DS2 (and DS70 and its descendants). *H. volcanii* is one of the very few archaea for which genetic tools are available, and it is commonly used to study archaeal cell biology (35–37). To the best of our knowledge, there is currently no other virus available that infects this species (38). This new model virus–host system allows analysis of the influence of a chronic life cycle on basic cellular processes such as genome replication and cell division (37, 39) in a prokaryotic organism in detail. First insights reveal a surprisingly high virus release and virus-to-host ratio (VHR), while having little impact on the overall fitness of the host. Moreover, upon infection, Haloferax volcanii pleomorphic virus 1 (HFPV-1) induces specific changes in the transcriptional program of *H. volcanii*, particularly downregulating transcription of genes in endogenous provirus regions of the host. The latter suggests that virus–virus interactions play a key role in the infective cycle of HFPV-1, which is supported by experiments showing that the presence or absence of one of these proviruses heavily modulates the outcome of infection.

Furthermore, to date, HFPV-1 is the only pleolipovirus that is capable of infecting a wide range of hosts across diverse haloarchaeal clades, thereby exhibiting promising traits for development as a genetic tool for diverse archaea, including those that cannot be genetically manipulated yet.

Experimental Procedures

Sampling Sites and Culture Conditions. Sediment samples were collected from Lake Tyrrell (35°20′38″S, 142°50′00″E) on December 23, 2018 (Department of Environment, Land, Water and Planning, Victoria, Australia, permit number 10008945) and kept at 4 °C until further use. For the isolation of viruses, enrichment cultures were established. Approximately 500 mg of sediment were completely dissolved in 100 mL of rich medium (Hv-YPC media) (40), supplemented with 1 mL of trace element solution and 3 mL of vitamin solution [21], referred to as Hv-YPC+. Dissolved samples were incubated aerobically at 45 °C with constant agitation (120 rpm) for 14 d. Ampicillin and kanamycin were used to prevent bacterial growth (final concentrations of 0.1 and 0.03 mg/mL, respectively).

Isolation and Purification of Viruses. Enrichment cultures were centrifuged at $4,500 \times g$ for 45 min to pellet the cells. The supernatant was recovered, and viruses were subsequently precipitated with polyethylene glycol (PEG) 6000 (10% wt/vol final concentration) and incubation at 4 °C overnight. Then, viral preparations were collected by centrifugation ($13,000 \times g$, 45 min, 4 °C). Pellets were resuspended in 18% buffered salt water (BSW) (180 g of NaCl, 25 g of MgCl2, 29 g of MgSO$_4$, and 5.8 KCl per L), sterile filtered (pore size 0.2 μm), and used for plaque assay and, after another filtration (pore size 0.2 μm), in liquid culture infection assays. Viral preparations were screened for viruses infecting *H. volcanii* DS2 (German Collection of Microorganisms and Cell Cultures GmbH). Briefly, 5×10^9 cells of *H. volcanii* were grown in Hv-YPC+ media at 45 °C, harvested from an exponential phase growing culture (optical density at 600 nm of one), mixed with 20 μL of viral suspension from each enrichment, and incubated for 2 h at room temperature to allow viral adsorption. Then, treated cells were either 1) used for plaque assay by mixing with 10 mL of top layer agar (base agar 10g/L and top layer 4 gr/L), plating, and incubating for a week at 28 °C or 45 °C or 2) used to inoculate a 100-mL liquid culture that was monitored by measuring optical density changes. No plaque formation was observed, but one liquid culture with a slight growth retardation was chosen for further analysis. Virus particles were isolated from culture supernatants as described above for enrichment cultures. For infection assays, the virus solution was filtered two times (pore size 0.2 μm), and cell contamination was excluded by inoculating the virus solution into media and incubation for 2 wk to exclude growth. For genomic DNA extraction, the virus solution was treated with 20 μL of DNase I and 10 μL of RNase to reduce host genomic DNA contamination, and was further purified on a CsCl (0.45 g CsCl/mL 15% BSW) density gradient (38,000 rpm for 22 h, 4 °C, SW 41 Ti Swinging-Bucket rotor, Beckman & Coulter). Bands containing virus particles were extracted with a syringe, diluted in one volume of 18% BSW, and reprecipitated with PEG (final concentration 10%, 4 °C, overnight), and the resulting pellet was washed two times with 18% BSW before DNA extraction. DNA was extracted using genomic DNA extraction kit (Bioline) according to the manufacturer's instructions. Virus particles were observed by transmission electron microscopy (TEM). Virus-containing solution was adsorbed for 5 min to carbon-coated copper grids (company) and stained for 1 min with 2% uranyl acetate (wt/vol in water). Electron micrographs were generated

using an FEI Tecnai F20 S-TWIN or JEM2100 Plus at 200-kV acceleration voltage.

Analytic Digest of Genomic DNA, Genome Sequencing, and Protein Content Analysis. For analytic digestion of genomic DNA, 1 μg of DNA was digested with restriction enzyme *Hind*III (37 °C, 1 h). To determine methylation patterns, genomic DNA was digested with *Dpn*I and *Bsp*143I (37 °C, 1 h). To search for single-stranded interruptions, the genome HFPV-1 DNA was digested with *Bal*31 and Exonuclease III (30 °C for 10 min). All products were separated on 1% agarose gels and visualized by staining with SYBR Safe (Invitrogen).

For DNA sequencing, libraries were prepared from purified DNA using FS DNA Library (NEBNext Ultra), and samples were sequenced with Illumina HiSeq2500 (Max Planck-Genome-Centre), with paired end 2×250 bp (paired end) read length. The sequenced reads were quality trimmed using the software Cutadapt (41), with a minimum quality of 30 and a minimum length of 50 (-q 30, -m 50). Subsequent assembly of high-quality reads was performed with assembler SPAdes v3.13.1 from ref. 42. Contigs coverage was calculated using BBmap v38.06 (43) with a minimum identity of 99% (minid = 0.99). Protein prediction was performed using Prodigal (44). Functional annotation of predicted proteins was done with the software package HH-suite3 (45) against the PDB70 database (release pdb70 200108) and the Big Fantastic database (BFD) (46). The genome is available in the National Center for Biotechnology Information (NCBI) database under accession number OM621814. Protein content analyses of in-solution sample preparation were performed using mass spectrometry (MS) as described in ref. 47. For gel-separated samples, the protein profiles were analyzed by using a Tris-Glycine sodium dodecyl sulfate polyacrylamide gel electrophoresis (SDS/PAGE) gel electrophoresis (12% acrylamide in resolving gel). Gels were stained with fast Coomassie staining (50% ethanol, 10% acetic acid, 0.5% wt/vol Coomassie Blue). The protein content of selected regions or the entire gel lane line separated into four to six slices were in-gel reduced with Dithiothreitol (DTT), alkylated with iodoacetic acid (IAA), and digested overnight with trypsin (Promega). Resulting peptide mixtures were extracted twice by exchange of 5% formic acid (FA) and acetonitrile and dried down. Peptides were resuspended in 25 μL of 5% FA, and a 5-μL aliquot was analyzed by liquid chromatography–MS/mass spectroscopy (LC-MS/MS) on a nano-ultra-high performance LC (nano-UPLC) system interfaced to a Q Exactive HF Orbitrap or an LTQ Orbitrap Velos mass spectrometer (Thermo Fischer Scientific). The nano-UPLC was equipped with an Acclaim Pep-Map100 C18 75-μm internal diameter (i.d.) $\times$ 20-mm trap column and a 75 μm $\times$ 15 cm analytical column (3 μm/100 A, Thermo Fisher Scientific). Peptides were separated using an 80- or 180-min linear gradient for gel bands and unfractionated samples, respectively; solvent A was 0.1% aqueous FA, and solvent B was 0.1% FA in neat acetonitrile. Spectra were acquired using the Data-dependent acquisition (DDA) method and Top 20 approach; lock mass set on $m/z = 445.1200$. Three blank runs were performed after each sample analysis to minimize carryover.

All MS/MS samples were analyzed using Mascot (Matrix Science; version 2.2.04). Mascot was set up to search against the *H. volcanii* DS2 and HFPV-1 predicted proteins, assuming the digestion enzyme trypsin. Mascot was searched with a fragment ion mass tolerance of 0.025 Da and a parent ion tolerance of 5.0 PPM; label: $^{13}C_6\,^{15}N_2$ of lysine; label: $^{13}C_6\,^{15}N_4$ of arginine, oxidation of methionine, acetyl of the n-terminus, carbamidomethyl of cysteine, and propionamide of cysteine were

specified in Mascot as variable modifications. Scaffold (version Scaffold_4.10.0, Proteome Software Inc.) was used to validate MS/MS-based peptide and protein identifications. Peptide identifications were accepted if they could be established at greater than 91.0% probability by the Peptide Prophet algorithm (48, 49) with Scaffold delta-mass correction. Proteins that contained similar peptides and could not be differentiated based on MS/MS analysis alone were grouped to satisfy the principles of parsimony. Only proteins with more than two unique peptides were considered in downstream analyses as quality control, while relative abundances were calculated by averaging the c values of biological triplicates.

Virus Infectivity and Kinetics. To study the life cycle, cultures of *H. volcanii* were synchronized using an adaptation of the "stationary phase method" (50). For this, a single colony was picked in liquid culture and grown in Hv-YPC+ media up to an optical density at 600 nm (OD_{600}) $\approx$ 1. Then a 20-fold dilution step in fresh media was performed (final OD_{600} = 0.05), and cultures were then regrown up to an OD_{600} of one. Iterative dilution and growth of the culture were repeated three times before considering a culture synchronized. For infection with HFPV-1, 1×10^9 cells ($OD_{600} \approx 1$) from synchronized cultures were collected by centrifugation, resuspended in 500 μL of fresh media, and infected with HFPV-1 virus with a multiplicity of infection (MOI) of 10. After incubation (2 h, room temperature), cells were transferred into liquid cultures, and growth was monitored by optical density (OD_{600}) every 6 h. Viral titer was quantified for free and intracellular virus by qPCR. Briefly, samples of 1 mL in biological replicates were collected and pelleted (11,000 $\times$ *g*, 10 min, room temperature). Supernatants were recovered, and PEG 6000 was added to a 10% wt/vol final concentration and stored at 4 °C, and virus particles were precipitated as described above. Cell pellets were washed two times with 1 mL of fresh Hv-YPC+ media, flash frozen with liquid N_2, and stored at −20 °C upon DNA or RNA extraction. DNA was extracted using a genomic DNA extraction kit (Bioline) according to the manufacturer's instructions. Long-term cultures were established by diluting infected cultures every 7 d. Infection was assessed by PCR with specific primers targeting the genome sequence of HFPV-1 (TyrVUF 5′-acgaacgagaacaccgacc-3′ and TyrVUR 5′-tgatgacgaatccaacgagcag-3′). Each PCR was performed with the Q5 High-Fidelity DNA Polymerase (New England Biolabs) and contained 0.02 U/μL polymerase, primer concentration of 0.1 μM for both forward and reverse, 1× of Q5 Reaction Buffer, and 1× Q5 High GC Enhancer. The following program was used: 5 min at 95 °C, followed by 35 cycles of 30 s at 95 °C, 30 s at 68 °C for annealing, and 30 s at 72 °C for elongation. Results were visualized in 1% agarose gels stained with SYBR Safe (Invitrogen).

Quantification of *H. volcanii* and HFPV-1 genome copy number (gcn) were carried out using a CFX96 Touch Real-Time PCR (Bio-Rad Laboratories, Inc.) and the software CFX Manager Software. Host DNA polymerase II small subunit gene (HVO_0003) was amplified with a specific primer set (FpolB 5′-cccgaatcaggacgaagaac-3′ and RpolB 5′-atttgaggtgctcggagaac-3′). Each reaction (10 μL) contained 1× SsoAdvanced Universal SYBR Green Supermix (Bio-Rad) and 300 nM of each primer. For viral quantification, a primer set targeting the internal structural protein 3 was designed (FVP3 5′-ttgcgtacgcggtatctgtc-3′ and RVP3 5′-agcttctccgcatcgtcttt-3′). The following amplification thermal cycling program was used for both primer sets: 5 min at 95 °C, followed by 40 cycles of 30 s at 95 °C and 30 s at 68 °C, with readings taken between each cycle. Efficiencies of the assays

were 95 to 100%, with R^2 values ≥ 0.99 for all assays. The specificity of the qPCR was confirmed by unique signals in melting curves and gel electrophoresis of PCR products.

Transcriptomic Analyses. RNA extraction of frozen cell pellets in three biological replicates was performed with the Zymo Direct-zol RNA miniprep Kit (R2051). RNA concentration and integrity were assessed using nanodrop DS-11 Spectrophotometer (DeNovix) according to the manufacturer instructions. Ribosomal RNA (rRNA) was depleted prior to sequencing using the rRNA depletion Kit riboPOOL, for *H. volcanii*, siTOOLs Biotech. Libraries were prepared with library kit NEBNext Ultra II RNA Library Prep Kit for Illumina, and sequencing was performed on an Illumina HiSeq3000 sequencer, using sequencing kit, following a 1×150 run. Sequencing depth of the samples ranged from 4.3 million to 7.2 million reads (mean = 6.5 million, SD = 0.7 million reads). Raw reads were quality trimmed with Cutadapt (41), with a minimum quality of 30 and a minimum length of 50 (-q 30, -m 30), and all reads containing "N" bases were removed. Filtered reads were mapped to *H. volcanii* DS2 strain and HFPV-1 genome using BBmap v38.06 with an identity threshold of 99% (minid = 0.99). Differential expression analyses were performed with R package DESeq2 (51) and plotted using ggplots2 (52). Briefly, raw counts were normalized by sequencing depth and geometric mean (51), and differential expression was calculated comparing the differences in read counts between infected and uninfected cultures by each time point (with three biological replicates for the infected and two biological replicates for the controls). Genes with P values < 0.01, false discovery rates < 0.05 (p adjusted < 0.05), and a fold change of at least two times ($\log2FC \geq 1$ or ≤ -1) were considered differentially expressed (DE). Raw data were submitted to European Nucleotide Archive (ENA) under Project Number PRJEB50750.

Global Distribution and Alternative Hosts of HFPV-1. The viral genome was searched against the Integrated Microbial Genomes/virus (IMG/VR) database (53) using Basic Local Alignment Search Tool (BLASTn) (54), e value $< 10^{-5}$, to detect uncultivated relatives from metagenomes or previous isolates. Original sequencing read files (metagenome or host isolate sequencing projects) for each target were then retrieved from relevant BLAST hits (identity $\geq 70\%$ and query coverage $\geq 50\%$.). HFPV-1 presence in these samples was determined by read mapping using BBmap (minid = 0.95), and HFPV-1 was considered present when the genome had at least $\geq 75\%$ of genome length with $\geq 1\times$ coverage (55). Furthermore, to establish the geographical distribution of the virus, an additional BLAST against the Virus CRISPR Spacer Database from IMG/VR was performed. This database contains short spacer sequences retrieved from CRISPR-Cas arrays from isolated and metagenomic genomes deposited in the databases. Only BLAST hits with an e value $< 10^{-5}$ and identity $\geq 90\%$ were considered as true positives.

Host Range Assessment of HFPV-1. Eight different strains of haloarchaea were tested to determine the host range of HFPV-1 (*SI Appendix*, Table S1). Exponential phase cultures were infected with HFPV-1 with an MOI of ~10, following the same procedure aforementioned, and incubated at 28 °C with constant agitation (120 rpm). Growth kinetics were monitored through optical density, while cells were collected by centrifugation (10,000 × *g*, 10 min), washed two times with fresh media (to avoid false positives arising from free virus in the supernatant), and screened for HFPV-1 infection by PCR (see *Virus Infectivity and Kinetics*). PCR-positive strains were selected, viral particles were isolated from culture supernatants by PEG precipitation (as described

above), and HFPV-1 particle production was assessed by qPCR (see *Virus Infectivity and Kinetics*). In order to confirm infectivity, viral particles isolated from the supernatant of alternative hosts were used to infect virus-free *H. volcanii*. Infection was confirmed by PCR as previously described.

Transformation of *H. volcanii* with HFPV-1 Genomic DNA. Transformation of *H. volcanii* was carried out by using PEG 600 as described previously in ref. 56. Briefly, cultures of *H. volcanii* were grown to an OD_{600} of ~0.8 and then harvested by centrifugation (30 min 4,500 × *g*). The pellet was gently washed one time in 2 mL of spheroplasting solution (1 M NaCl, 27 mM KCl, 50 mM Tris·HCl, sucrose 15%) and then gently resuspended in 1 mL of spheroplasting solution. The solution was chelated with 0.5 M (ethylenedinitrilo)tetraacetic acid (pH 8). Then four different concentrations of HFPV-1 genomic DNA were used for transformation (100 pg, 1 ng, 10 ng, and 100 ng DNA, respectively). Additionally, two genomic DNA samples of HFPV-1 that were treated with DNase and RNase (DNase I and RNase H, respectively; New England Biolabs) were used as controls. After addition of DNA, 250 μL of 60% PEG_{600} was added and mixed gently, and incubated at room temperature for 1 h. Then, cells were washed two times and transferred into a regeneration solution (Hv-YPC+ media with 15% sucrose) for 3 h at 28 °C before transfer into liquid culture. Successful infection was assessed by PCR and isolation of virus particles from culture supernatants as described above (host range assessment).

Knockout Mutant Strains Generation and Determination of HFPV-1 Infection. Transformation and construction of deletion mutants in *H. volcanii* H133 ($\Delta pyrE2$ $\Delta trpA$, $\Delta leuB$, and $\Delta hdrB$) based on selection with uracil were performed as described previously (57). Plasmid construction was done by classical restriction enzyme-based molecular cloning. Inserts were amplified from wild-type (DS70) genomic DNA (using genomic DNA extraction kit: Bioline, according to the manufacturer's instructions) via PCR using Phusion polymerase (NEB). All restriction endonucleases used were purchased from NEB. Restriction enzyme digestions and PCR were performed according to the manufacturer's protocols. Provirus Halfvol 3 (ΔHVO_1422 to HVO_1434) was generated by first generating a deletion mutant of HVO_1434. Two fragments were generated using the following primer and restriction enzymes: A1434up5 (*Not*I) 5′-aacgcggccgcagtcgttgatggcgttgccc-‘3, A1434up3 (*Xba*I) 5′-aactctagactccgagagaccgcacgcg-‘3 and A1434down5 (*Eco*RI) 5′-aacgaattcaggaacctaccctgcctggt-‘3, A1434down3 (*Hind*III) 5′-aacaagcttagcgaactcgcgcatcagag-‘3. Fragments were cloned into pTA131 (57) and transformed into *H. volcanii* after isolation from dam^-/dcm^- competent *E. coli* cells (NEB). The remaining part of provirus Halfvol 3 was deleted in ΔHVO_1434 after cloning the fragment generated before with A1434up5 and A1434up3 and a fragment generated using primers A1422down5 (*Eco*RI) 5′-aacgaattccgacatatccgaacgcgagag-‘3 and A1422down3 (*Hind*III) 5′-aacaagcttgtgttccgatggccgtgac-‘3 into pTA131. The construct was demethylated by isolation from dam^-/dcm^- competent *E. coli* and transformed into ΔHVO_1434, and, after selection with uracil, pop-out was performed as described. The resulting ΔHVO_1422 to HVO_1434 deletion strain was confirmed by PCR (Halfvol3F 5′-ccgatgtactgaccctgac-‘3, Halfvol3R 5′-agacataccccgtactgttc-‘3) and Sanger sequencing of the resulting PCR product. Virus infectivity on the provirus mutant strain was determined as described above for wild-type *H. volcanii* (*Virus Infectivity and Kinetics*). Experiments were performed in three biological replicates, and the

parental strain was used as a wild-type control. Hv-YPC+ was supplemented with uracil (50 μg/mL), tryptophan (50 μg/mL), leucine (50 μg/mL), and hypoxanthin (40 μg/mL) to support growth.

Results and Discussion

Isolation of a Virus Infecting the Model Haloarchaeon *H. volcanii*.
The halophilic archaeon *H. volcanii* is widely used as a model organism for the study of archaeal cell biology and biochemistry and is one of few archaea with an extensive genetic toolset available (36, 58). A number of viruses infecting halophilic archaea have been isolated (17, 59); however, no virus was available for a model haloarchaeon that would allow a detailed study of virus–host interactions in halophilic archaea. To isolate a virus specifically targeting *H. volcanii*, enrichment cultures in media specified for *H. volcanii* at optimal growth temperature of *H. volcanii* were established, using samples taken at hypersaline Lake Tyrrell, Australia (60). Virus-containing supernatants were generated from enrichment cultures and tested on *H. volcanii*. Growth retardation was observed in one of the treated *H. volcanii* cultures, and DNA containing virus-like particles (VLPs) were retrieved from the supernatant. TEM of the samples revealed the presence of nonsymmetrical pleomorphic particles, with sizes ranging from 50 nm to 80 nm (Fig. 1*A*), and represents the only virus isolated for this species; thus we named it Haloferax volcanii pleomorphic virus 1 (HFPV-1).

Genomic Characteristics of HFPV-1 and Taxonomic Classification.
Analytic digests of HFPV-1 genomic DNA revealed a double-stranded DNA genome with single-stranded interruptions (*SI Appendix*, Fig. S1). The presence of a conserved DNA motif that precedes single-stranded discontinuities in the genome of Halorubrum pleomorphic virus 3 (HRPV-3) (61) was in silico identified in HPFV-1 genome (GCCCA motif $n = 3$); however, experimental evidence is further needed to confirm that it is a common trait in HFPV-1 as well. Meanwhile, no dam methylation was detected on the genome of HFPV-1 (Fig. 1*B*). Illumina sequencing and genome assembly yielded a contig of 7,924 base pairs (bp) with overlapping ends, which circularizes to a single molecule of 7,869 bp and encodes for 11 open
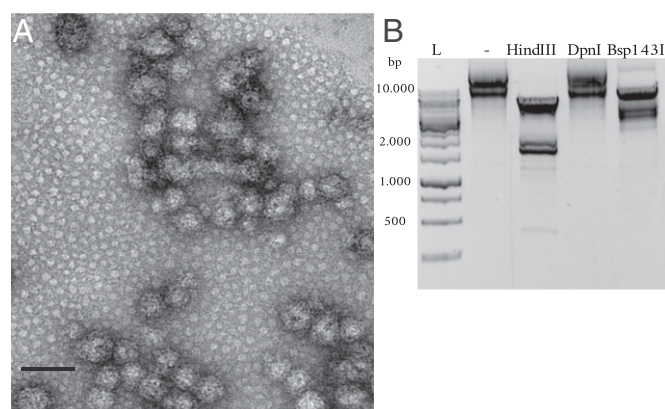
Fig. 1. (*A*) Transmission electron micrographs of HFPV-1. Viral concentrates were sterile filtered (0.2 μm) and purified through CsCl density gradients. Particles were negatively stained with uranyl acetate and imaged at 200 kV on an FEI Tecnai TF20. (Scale bar, 100 nm.) (*B*) Analytic restriction digest of HFPV-1 genomic DNA with different restriction enzymes. Molecular weight size marker (L) is shown (gene ruler 1 kb; DNA ladder, Thermo Fisher Scientific). Untreated (-) and restriction digestion with enzymes *Hind*III, *Dpn*I, and *Bsp*143I. DNA was separated on 1% agarose gels and stained with SYBR Safe (Invitrogen) at a final concentration of 1×. Data represent one sample of three biological replicates. The restriction digest patterns were observed in four repetitions.

reading frames (ORFs) (*SI Appendix*, Fig. S2). The average GC content of HFPV-1 is 59.3%, which is significantly lower than the GC content of the main chromosome of *H. volcanii* (66.6%), and more similar to *H. volcanii* plasmids pHV1, pHV2, and pHV4 (56%, 55.5%, and 61.7% respectively) (62).

The genome of HFPV-1 displayed no significant similarity at the nucleotide level with any previous viral isolate, while low identity values at the protein level were observed when compared with members of the *Pleolipoviridae* family (Fig. 2). Further comparison against multiple viral databases (see *Experimental Procedures* for details) revealed the presence of two putative structural proteins (ORF2 and ORF4) homologous to the spike proteins of *Halogeometricum sp.* pleomorphic virus 1 HGPV-1 (63), a member of the *Betapleolipovirus* genus, although the similarity was rather low (identity = 45%). ORF3 has little similarity to any known protein and only has a homolog in HGPV-1 among related viruses, but its function remains unknown. Three other proteins (ORF5, ORF6, and ORF7) presented a significant homology to the conserved core cluster of proteins within the *Pleolipoviridae* family (Fig. 2). ORF7 is proposed to have NTPase activity, and both ORF6 and ORF7 are predicted to have transmembrane domains, but their function and role in the infective cycle of the virus has not been characterized. Further assessment of the hypothetical proteins encoded by HFPV-1 using hidden Markov models showed that two predicted proteins, ORF1 and ORF9, were similar to transcriptional regulators (probabilities of $P = 99.44$ and 84.96, respectively).

No replication protein could be identified in the genome of HFPV-1. However, it possesses a predicted DNA binding protein (ORF10, $P = 91.77$) at the position where related pleolipoviruses encode their predicted replication protein (Fig. 2). This is of particular interest because, thus far, the taxonomic affiliation of the members of the *Pleolipoviridae* normally correlated with their proposed replication mechanisms. While the alphapleolipoviruses are thought to replicate via a rolling circle replication endonuclease (61), and the gammapleolipoviruses possess a protein-primed family B DNA polymerase (pPolB polymerase) (59), the betapleolipoviruses, whose members are the ones with highest homology to HFPV-1, present a conserved homolog of an uncharacterized replication protein (Rep protein; Fig. 2) (64). The lack of the conserved replication protein present in all related viruses and the lower identity values at the protein level suggest that HFPV-1 is a rather divergent member of the *Betapleolipovirus* genus.

Protein Composition of HFPV-1 Particles Differs from Closely Related Viruses, and Particles Are Stable at a Wide Range of Salt Concentrations.
MS of virus particles confirmed the presence of ORF4, the predicted spike protein, as the most abundant structural protein present in the virus particles (average peptide count = 1,700; Dataset S1). Interestingly, no signal was detected for the predicted internal membrane protein ORF2, neither by individual SDS/PAGE band sequencing (*SI Appendix*, Fig. S3) nor by MS of whole purified viral particles, despite presenting trypsin digestion sites. This suggests that, unlike for its closest relative HGPV-1, this protein is not within virions, or another method such as N-terminal sequencing would be required to detect it. Additionally, four other proteins, ORF3, ORF5, ORF6, and ORF7, were detected in virions (Dataset S1). While no function could be predicted for ORF3 and ORF5, we detected transmembrane domains in ORF6 and ORF7. However, whether these proteins are involved in virion assembly or the infection process remains to
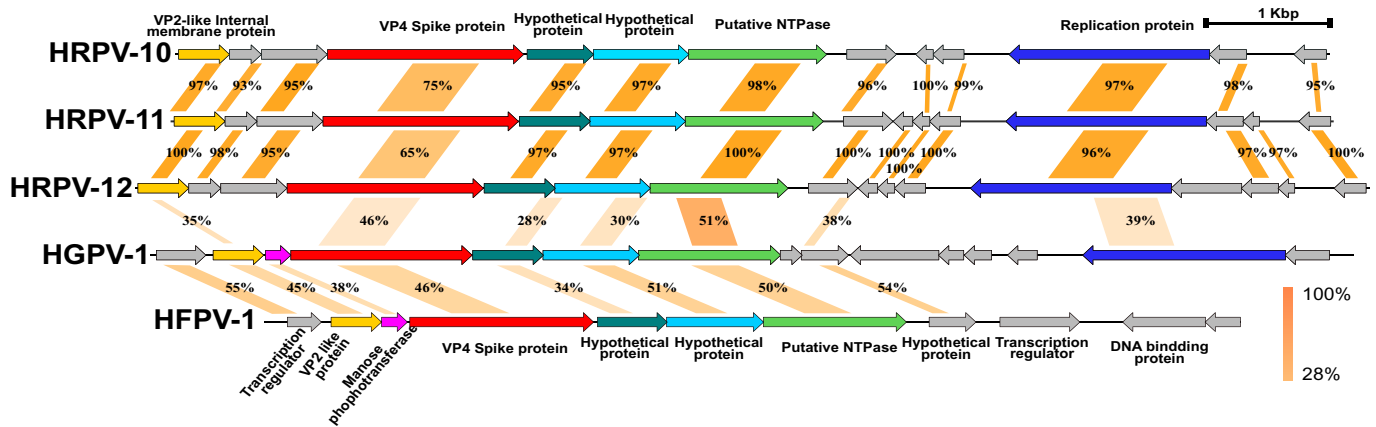
Fig. 2. Genome comparison of HFPV-1 with closest related pleolipoviruses. Homolog genes are indicated with the same colors. Vertical colored bars represent the percentage of identity between protein pairs. HRPV-10, HRPV-11, and HRPV-12: Halorubrum pleomorphic viruses; HGPV-1, Halogeometricum pleomorphic virus 1.

be elucidated. Noteworthy is that a number of host-encoded proteins were also detected in the viral preparations in significant amounts, such as the S-layer protein and several transporters (Dataset S1). However, the detection of these proteins in the preparations can be attributed to membrane vesicles present in the sample. These vesicles are naturally produced by *H. volcanii* independently of viral infection, and they copurify with HFPV-1, due to their similar physical properties.

Transformation of uninfected *H. volcanii* cells with purified HFPV-1 DNA generates a successful infection, indistinguishable from the infection with virus particles (*SI Appendix*, Fig. S4); we therefore conclude that none of the viral proteins is crucial for initiation of the virus life cycle once the virus DNA has entered the host cell.

Sensitivity to different conditions was assessed through a spot test (65), revealing that viral particles remain stable in 18% BSW at 4 °C for over a year. Infectivity was maintained upon freezing with liquid nitrogen after 2 mo; however, samples stored at −20 °C lost their infectivity within a day. Assessment of thermal stability through spot tests revealed that particles remain infective after 1-h incubation at 50 °C but are inactivated at 60 °C and above. Particles also exhibited remarkable versatility under osmotic stress, remaining infective in salt concentrations ranging from 5 to 25%. Furthermore, the ability to generate an infection by transformation of purified virus DNA provides an advantage for long-term storage and highlights the potential of HFPV-1 to be developed into a genetic tool.

HFPV-1 Causes Only a Minor Impact on Host Growth Despite High gcn and High Viral Titers. Infection of *H. volcanii* cells in an exponential phase with HFPV-1 with an MOI of 10 caused only a slight growth retardation of the host in liquid culture (Fig. 3). No decrease in the turbidity of the media was observed, well into stationary phase, supporting the nonlytic nature of HFPV-1 infection. Long-term experiments revealed that the virus and the host form a stable relationship in liquid cultures, where viral infection and release is detectable by PCR for at least 3 mo (weekly dilution), without the emergence of resistant cells nor extinction (complete lysis) of the host (*SI Appendix*, Fig. S5).

Consequently, during plaque assays with purified viral particles, no zones of cell lysis were observed, regardless of temperature (28 °C to 45 °C) and salt concentration (15 to 22%). Therefore, the viral titer was determined by measuring viral gcn

in the supernatant of liquid cultures by qPCR. Virus particles could be first detected in culture supernatants at 24 h post infection (h p.i.). Subsequently, an exponential increase in the concentration of free virus in the supernatant was observed, reaching up to 1×10^{10} gcn per mL^{-1} 84 h p.i. (Fig. 3). Assessment of the intracellular viral titer, and subsequent calculation of the VHR, unveiled a high number of viral genomes within each cell, with VHR values up to ~10^3 at 72 h p.i. (average VHR = 977.5; *SI Appendix*, Fig. S6). However, *H. volcanii* is a polyploid organism, and can have up to 20 copies of the genome during exponential phase (66); therefore, the total number of viral genomes within each cell could be severely underestimated.

Transcriptional Profile of the Viral Genome during Infection. So far, most studies that investigated changes in gene expression during viral infection in prokaryotes have focused on the impact of the infection by lytic viruses (67). However, little is known about how the transcriptional program changes upon a long-term chronic infection in a prokaryotic organism. HFPV-1 produces a highly stable and reproducible infection cycle in *H. volcanii,* and is therefore a good model for analyses of infected populations.
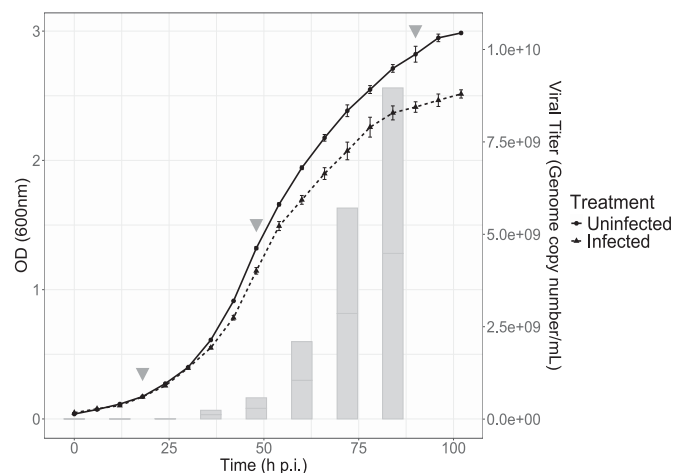

Fig. 3. Virus life cycle: growth curve of uninfected (black circles) and infected (black triangles) *H. volcanii* DS2 cultures. Error bars represent the SD for biological triplicates on both treatments. Gray bars represent the number of free virus particles in the supernatant of liquid cultures, assessed through qPCR using specific probes targeting the HFPV-1 genome. Inverted gray triangles indicate time points chosen for transcriptomic analyses.

In order to shed light on the nonlytic life cycle of HFPV-1, we took samples from synchronized infected and control cultures at three different stages of the viral life cycle (Fig. 3): 1) lag phase, from 0 h to 24 h p.i., with little to no virus release and by growth rate undistinguishable to the uninfected cultures; 2) exponential phase, from 24 h to 72 h p.i., characterized by growth retardation, continuous release of virus particles, and the highest numbers of intracellular virus genomes; and 3) stationary phase, from 72 h to 102 h p.i., characterized by media exhaustion and limited growth, while reaching the highest viral titers in the supernatant. The respective representative samples were taken in three biological replicates at 18, 48, and 90 h p.i. for lag, exponential, and stationary phases, respectively.

Transcriptomic analyses revealed that all predicted viral genes are expressed across the three different growth phases, comprising increasing portions of the total transcriptome as the infection spreads, from an average of ∼2% in lag phase to ∼7% and 16% during exponential and stationary phases, respectively (Dataset S2). ORF4, which encodes the structural spike protein, along with the ORF10, a DNA binding protein, are the most highly expressed virus genes (average transcripts ≈ 150,000). Interestingly, the ORF10 location in the genome of HFPV-1 matches the genomic location of the proposed replication protein in other *Betapleolipoviruses* but shares no homology with these replication proteins or any other known protein. The position in the genome, together with the high expression levels, and the lack of any other recognizable replication-associated gene, suggests that ORF10 could be a representative of an undescribed family of replication proteins. Additionally, the second predicted structural protein, ORF2, is the third most highly expressed gene. However, the protein product was not detected in purified virus particles, despite the fact that it has four predicted transmembrane domains, and its role in particle formation and infection remains unknown.

Global Pattern of Host Metabolic Takeover in *H. volcanii* Is Phase Dependent. Global analysis of the transcriptional program of the host showed that the three defined phases of infection have remarkably different profiles, with 1,049 genes being DE at least at one of the three phases. Given that the transcriptional profile of each of the growth stages was extremely different, further comparisons to establish the DE genes were always performed between infected and uninfected controls for each time point independently.

The largest number of DE genes was observed during the exponential phase (887 DE genes), with most of the genes being down-regulated (597 genes), meanwhile, the lag phase exhibits the least changes, with only 171 DE genes. During this phase of infection, only relatively few changes in the transcriptomic profile of *H. volcanii* were observed, with 159 genes being up-regulated and only 12 genes being down-regulated (Dataset S2). The two top-ranked overexpressed genes are proteins that encode a DoxX domain (HVO_0763 and HVO_A0548), and, while their specific function in *H. volcanii* remains unknown, characterized members of this protein family are associated with oxidoreductase complexes, specifically linking radical detoxification with thiol homeostasis in *Mycobacterium tuberculosis* (68). Notably, a number of universal stress proteins containing the UspA domain are consistently overexpressed. These small cytoplasmic proteins are generally overexpressed when the cell is exposed to stress agents in an unspecific manner (69). In addition, several oxidoreductase genes, electron carriers, and halocyanines (e.g., HVO_2150, HVO_1119), as well as the RpaB2 gene (HVO_0291), were also up-regulated. Interestingly, the

single-stranded DNA-binding protein HVO_0291 has been shown to be one of the most highly up-regulated genes in *H. volcanii* upon exposure to H_2O_2 (70), further suggesting that the cells are undergoing oxidative stress during viral infection. Conversely, no significant up-regulation of any of the known specific immune response pathways was identified (71), with only a distant homolog to an RNase protein being up-regulated (HVO_1114), which could potentially target viral transcripts.

Interestingly, two groups of different transcriptional regulators modulating carbon metabolism appear to be up-regulated, with two genes belonging to the IclR family (HVO_B0040 and HVO_A0527), which regulate different carbon–related pathways (72), and one to the DeoR family (HVO_1501), which is commonly a repressor of sugar metabolism (73). The increase in the expression of these general carbon repressor-like regulators could be the reason for the subsequent growth retardation and may help hijack resources for virus production.

All together, the data largely suggest that, while the cells are enduring some degree of oxidative stress, which arises from the metabolic imbalance generated by the viral infection, the viral genome manages to remain hardly noticeable, thus avoiding triggering any major host defense mechanism at this stage of infection. The latter could be related to the absence of dam methylation on the viral genome, which allows it to escape primary host defense mechanisms against exogenous DNA.

HFPV-1 Induces a Massive Down-Regulation of the Host Transcriptome during Exponential Phase. The exponential phase presents a radically different landscape compared to the earlier stage of infection. This is highlighted by a massive transcriptional down-regulation of 597 genes, more than doubling the up-regulated ones (290 genes). This general down-regulation is, in itself, unusual when compared to previously reported studies on viral takeover of host metabolism in prokaryotes. Research in lytic virus-induced transcriptional changes carried out in *Sulfolobus* showed a trend of little to no down-regulation (74, 75). An exception is the case of the lytic virus SIRV2, infecting *Sulfolobus islandicus*, which was reported to have between 30% and 50% of the host genome differentially expressed during infection (76). However, the number of down-regulated genes is approximately the same as the number of up-regulated genes, and the magnitude of increase in transcription of the up-regulated genes was much higher than the decrease in the down-regulated genes (76). Intriguingly, during the infection of *Sulfolobus solfataricus* with the nonlytic virus SSV2, only around 5% of the genome was reported to be differentially expressed, with around 80 genes down-regulated (77, 78), which is considerably lower compared to the impact of HFPV-1. Similarly, microarray analyses of the nonlytic filamentous phage M13 that infects *E. coli*, one of the few examples of persistent infections in bacteria, also showed that only a small proportion of the genes are differentially expressed upon infection (79). In conclusion, to our knowledge, HFPV-1 generates one of the largest overall transcriptional down-regulations induced by a virus infecting archaea, and poses intriguing questions on how this relatively simple virus, encoding only 11 genes, is capable of establishing a successful and long-term infection.

In terms of cluster of orthologous genes (COG) functional categories, the most DE genes are found in the amino acids metabolism and transport (E), with 122 DE genes (112 down-regulated and only 10 up-regulated). Within this category, the most significant changes are observed for an ABC-type transport system for branched chain amino acids and dipeptides, which show up to a 34.2- to 48.5-fold decrease (HVO_0899,

HVO_0900, HVO_2801, and HVO_0901). Other categories such as energy production and conversion (C), with 82 DE genes (65 down-regulated and only 17 up-regulated), and inorganic transport and metabolism (P), with 69 DE genes (54 down-regulated and only 15 up-regulated), are strongly down-regulated (Fig. 4). In the case of energy metabolism, several NADH dehydrogenase complex components (e.g., HVO_0980, HVO_0981, and HVO_0982), as well as subunits of the A-type ATP synthase (HVO_0313, HVO_0315, and HVO_0316), are also down-regulated in a range of 3.7- to 4.6-fold change. The latter is likely to result in a disruption of the recycling of reductive power and ATP generation, which translates into less available energy for the cellular metabolism and could explain the observed growth retardation. Interestingly, genes involved in cell division exhibited a more moderate down-regulation, with only one of the essential proteins for cell division in *H. volcanii*, FtsZ2, that primarily participates in the constriction mechanism (37, 80), showing lower levels of expression (3.2-fold change), while other essential proteins like FtsZ1 or SepF are not differentially expressed. This is in contrast to STSV2, a nonlytic virus infecting *S. islandicus*, that leads to a strong down-regulation of cell division genes and a massive increase in cell size and DNA content (81).

Regarding cell motility, HFPV-1 generates an overall down-regulation of the archaellum machinery, with the archaellin A1 and A2 (HVO_1210 and HVO_1211) and the flagella-related proteins ArlCE, ArlD, ArlF, and ArlG (HVO_1213, HVO_1203, HVO_1214, and HVO_1215). These genes are proposed to be homologous to the FlaC/D/E complex, which is involved in transducing intracellular/extracellular signals that influence the activity of the flagellum. The FlaF gene, on the other hand, encodes for a b-sandwich protein that anchors the archaellum in the archaeal cell envelope by binding the S-layer protein, while the FlaG gene function is still unknown (82). However, despite those structural and signaling genes of the archaellum being down-regulated, analyses of electron micrographs of infected cells revealed that they possess an archaellum and are optically indistinguishable from uninfected cells (*SI Appendix*, Fig. S7). However, the actual mobility of the cells needs to be further investigated by motility assays.

The CRISPR-Cas System of *H. volcanii* Is Ineffective against HFPV-1 Infection. The CRISPR-Cas system is one of the most sophisticated and effective defense mechanisms known in archaea and bacteria (83), and it has been shown, previously, that it can be effective against other pleolipoviruses (84). *H. volcanii* encodes a single and fully functional CRISPR-Cas system of type I-B (71); however, it does not possess spacers targeting the HFPV-1 genome, and it does not prevent the development of a successful infection by HFPV-1. Upon infection with HFPV-1, several Cas proteins are down-regulated, with Cas8 (HVO_A0206), which is essential for the interference reaction, and Cas7, that mediates the sequence specificity of the defense system, enabling recognition by base-pairing with the invader DNA (71), being the genes subjected to the highest decrease (5.6-fold change). Meanwhile Cas6, which is essential for CRISPR RNA maturation but otherwise not required for the defense reaction, remains unaffected by the infection. Interestingly, the endonuclease Cas1 (HVO_A0211), which participates in new spacer insertion and acquisition, is down-regulated during exponential phase (2.0-fold change). The latter could explain why the host is not able to defend itself against infection with HFPV-1, given that the CRISPR arrays of *H. volcanii* do not have spacers against the genome of the virus, and the down-regulation of Cas1 could inhibit the process of acquisition of new spacers. Analysis of the transcriptomic data showed that there is no evidence for acquisition of new spacers, as there are no transcripts related to the CRISPR array that contain both viral sequences and repeats from one of the arrays, which supports this hypothesis.

Sustained Viral Production during Stationary Phase Despite Cellular Arrest. The transcriptional changes during the stationary phase followed a similar pattern to the one observed during exponential growth, highlighted by an exacerbated trend toward the down-regulation of host genes (216 down-regulated) (Dataset S2), although no down-regulation of any defense mechanism, including the CRISPR system, was observed. Interestingly, this massive down-regulation is concurrent with the largest proportion of viral mRNA (~16% of total mRNA) and consecutive to the highest values of intracellular viral load (VHR ≈ 10^3 at 72 h p.i.).
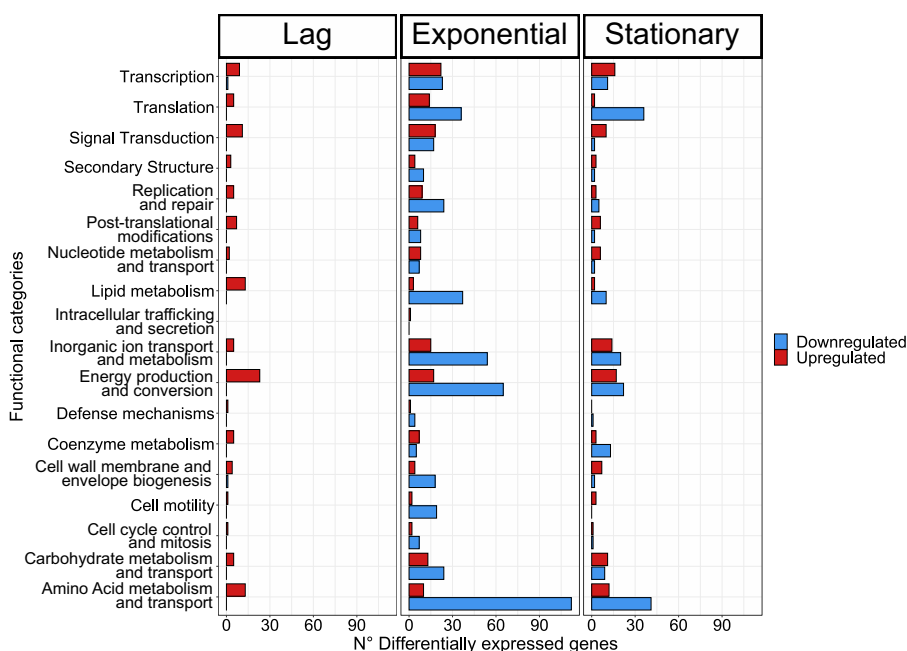

Fig. 4. Functional profile of differentially expressed genes. Bars represent the number of differentially expressed genes assigned to each particular functional category at a given growth stage, that is, lag, exponential, and stationary phases. Functional classification of *H. volcanii* genome was performed using the COG database. The colors of the bars indicate whether genes are up-regulated (red) or down-regulated (blue). Genes that were not assigned to any functional category are not displayed on the plot (for detailed information, see Dataset S2).

The latter suggests that, although cells enter division arrest, they remain highly productive viral factories, with the viral replication not being negatively affected by the lower nutrient availability and the CRISPR system remaining ineffective, despite the increasingly high amount of viral genetic material in the cells.

On the other hand, several genes that showed significant up-regulation, with more than a 30-fold increase in expression, are related to energy production and conversion (i.e., HVO_B0291, HVO_2411, HVO_1083, and HVO_2251) and two universal stress proteins (i.e., HVO_2337 and HVO_0401) (Dataset S2). Also, an acetate-CoA ligase (HVO_1000), which is a key enzyme that catalyzes the recycling of acetate to acetyl-CoA, to compensate starvation during stationary phase in *H. volcanii* (85), is threefold up-regulated. The data suggest that, upon infection with HFPV-1, the infected cells are forced to fulfill at least the energy requirements of the machinery dedicated to virus production.

The shutdown of numerous cellular metabolic functions as cells become quiescent could redirect most of the available resources to viral production, resulting in the highest proportions of viral RNA at 90 h p.i. Subsequently, as these alternative reservoirs are depleted, viral production is also halted, which would explain the decrease in the VHR values after 96 h p.i.

HFPV-1 Specifically Targets Provirus-Like Sequences in the Genome of *H. volcanii*. The genome of *H. volcanii* encodes at least two prophage regions that are likely defective, or temperate viruses from previous infections (Fig. 5). These proviruses are thought to have been maintained by the host because they encode an unknown evolutionary advantage. In this scenario, one of the reasons for the difficulties of isolating viruses infecting *H. volcanii* could be that the defective proviruses encode an unknown virus–virus exclusion mechanism. Evidence for the latter arose during in silico analyses of single-cell sequenced bacterial genomes, where cells with prophage sequences correlated with reduced coinfection events by other prophages (86). In *H. volcanii*, two of the identified proviruses can be related to members of the *Pleolipoviridae* family (87).

Remarkably, both prophage regions related to pleolipoviruses showed down-regulated genes during exponential and stationary phase (Fig. 5), with provirus region Halfvol1 having several genes among the highest ranked down-regulated genes. Particularly, HVO_0269 exhibited a fold change of more than 150× with respect to the uninfected cultures, the highest among any differentially expressed gene. The genes HVO_0268, HVO_0270, and HVO_0271 showed a very similar pattern, with decreases ranging from 40- to 60-fold change. Interestingly, there is sequence similarity, at the nucleotide level, with HFPV-1 in the downstream end of genes (HVO_0272 to HVO_0274, with a 77% similarity) which are also down-regulated (~10-fold change). However, there is no sequence similarity between the viral genome and the highest down-regulated genes (HVO_0269 to HVO_0271) or any of the other intergenic regions. Surprisingly, a single gene within this region exhibited the opposite trend (HVO_0262), being up-regulated in exponential phase at a 2.3-fold change. This suggests that the regulation of this genomic region rather depends on multiple promotors and/or mechanisms, viral, cellular, or both, that modulate, simultaneously, the gene expression.

The second prophage region (HVO_1422 to HVO_1434) seems to be a defective provirus related to alphapleolipoviruses, that also contains several genes with high homology to the
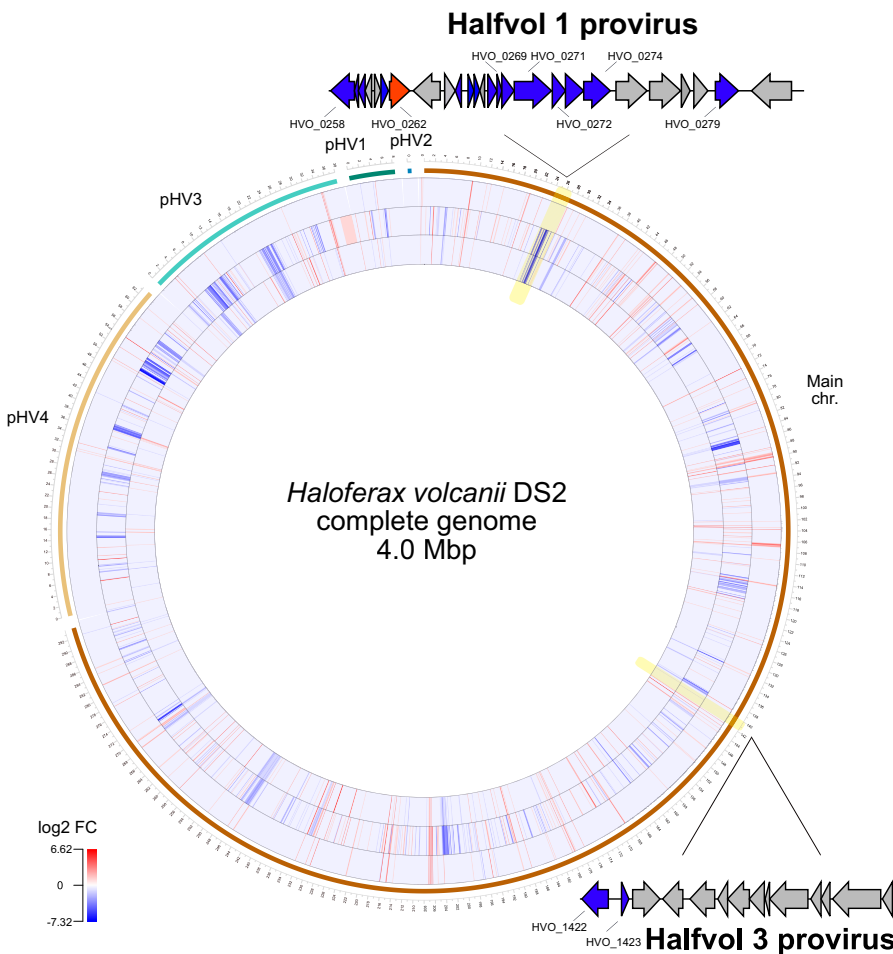

Fig. 5. Specific differential expression of prophage regions in the *H. volcanii* genome: heat map representation of gene expression profile of the host *H. volcanii*. The magnitudes of expression level changes are displayed as the $\log_2$ fold change (log2 FC) for up-regulated genes (red) and down-regulated genes (blue). Each heat map ring corresponds to one of the growth phases studied, that is: lag phase, outer ring; exponential phase, middle ring; and stationary phase, inner ring. Prophage regions phylogenetically related to pleolipoviruses are zoomed in, and genes that are differentially expressed during at least one growth phase are highlighted in blue (for details, see Dataset S2).

pHK2 plasmid from *Haloferax* sp. Aa2.2 (88). Two genes are down-regulated during the exponential and stationary phases, including an integrase (HVO_1422) and a transcriptional regulator (HVO_1423). Interestingly, HVO_1423 shows homology to the phage PhiH1 repressor protein, which can provide *Halobacterium salinarum* cells with immunity to infection by phiH1 virus (89, 90), and, potentially, could be playing a similar role in *H. volcanii*, by acting as a viral defense mechanism.

The third prophage region, which is proposed to be a degenerate provirus related to tailed viruses, exhibits a more patched pattern. Here, an integrase gene and unknown protein (HVO_2259 and HVO_2266) are moderately down-regulated (an approximately twofold to fourfold change), while the genes HVO_2254 and HVO_2255 are being overexpressed during the exponential phase. However, most genes remain unchanged upon viral infection.

Provirus Region Modulates the Outcome of HFPV-1 Infection.
Interactions between coinfecting viruses or between a virus and mobile genetic elements has been shown to have significant effects on viral fitness and life cycles (91, 92). Given the fact that genes from both proviral regions are down-regulated during infection with HFPV-1, we explored putative virus–virus interactions. To this purpose, a mutant strain lacking the provirus region Halfvol 3 was generated and subjected to infection with HFPV-1. Growth assays showed a much stronger growth retardation in the mutant strains lacking the provirus region (Fig. 6A). This suggests that, in the absence of this genome segment, HFPV-1 generates a more acute infection, which, in turn, suggests that the provirus region encodes one or more genes that interact with the primary infecting virus, and that mitigate the overall effects of the infection and decrease the capacity of HFPV-1 virus to generate additional copies of its genome. This is strongly supported by the differences in the observed VHR, where the infected mutant strain reaches up to 10 times higher VHR values than the parental strain (Fig. 6B). Interestingly, only two genes in this region are being down-regulated (HVO_1422 and HVO_1423, as described above). HVO_1423 as a potential repressor represents the best candidate to be responsible for inhibition of HFPV-1 infection, while, in return, the down-regulation of HVO_1422, the integrase, by HFPV-1 possibly prevents the excision of the provirus.

HFPV-1 Is a Promiscuous and Globally Distributed Virus. Previous studies have suggested that head-tail viruses from hypersaline environments have an unusually broad host range, as several viruses are able to infect multiple genera or secondary hosts isolated in distant locations (63, 93). However, the opposite trend has been observed for the members of the *Pleolipoviridae* family, as all isolates described, so far, were shown to be extremely species specific, infecting only a single host, commonly isolated from the same sampling site (11, 63).

Nonetheless, given that HFPV-1 was originally isolated from salt crust from Lake Tyrrell, Australia, and *H. volcanii* was isolated in the Dead Sea, we performed in silico analyses to identify potential additional hosts for HFPV-1. Particularly, when searching against the isolate and metagenome-derived CRISPR spacers database in the IMG/VR database, v.2.0 (53), we identified 10 spacers that were significant matches against the HPFV-1 genome, with identities ranging from 97 to 100% and an average length of 36 bp (Dataset S3). All of the spacers derived from sequenced genomes of previously isolated *Haloferax* species (i.e., *H. lucentense*, *H. denitrificans*, *H. alexandrinus*, and *H. massiliensis*), while no match was detected in the metagenomics-derived sequences. Furthermore, assessment of 59 genomes of previously sequenced *Halobacteria* isolates in Becker et al. (94) revealed that the genome of HFPV-1 could be detected in 9 of them, using previously described thresholds for viral detection in genomic data (read mapping identity $\geq$ 95%, genome coverage $\geq$ 75%) (55). This suggests that the isolates were likely infected with HFPV-1 or a closely related variant at the time of isolation, but the infection went unnoticed. These isolates belong to multiple genera (i.e., *Haloferax*, *Natronococcus*, *Halococcus*, and *Haloterrigena*; *SI Appendix*, Table S2), and indicate a wide host range of HFPV-1.

Hence, we assessed the host range of HFPV-1 under laboratory conditions using a collection of previously isolated haloarchaea. This yielded several species that exhibited susceptibility to infection by HFPV-1, while also being able to produce consistently viral progeny and generating a chronic infection similar to the one observed in *H. volcanii*. Surprisingly, the susceptible hosts included related genera within the *Haloferacaceae* family (i.e., *Haloquadratum* and *Halorubrum*), and also crossed higher taxonomic rank, infecting a member from a different family (i.e., *Haloarculaeace*) (*SI Appendix*, Table S1 and Fig. S8). Quantification of HFPV-1 gcn in culture supernatants from these alternative hosts reveled that *H. volcanii* produced the highest number of virus particles among the assessed organisms(2.542×10^{11} copies per mL^{-1} per OD_{600}^{-1}; *SI Appendix*, Table S3). Interestingly, another member of the same family the square-shaped *Haloquadratum walsbyi*, for which no virus has been yet isolated, displayed the second highest efficiency of viral production (2.808×10^{10} copies per mL^{-1} per OD_{600}^{-1}). Meanwhile, the most distantly related organism, *Haloarcula japonica* (*Haloarculaeace*), exhibited the lowest efficiency (2.730×10^{8} copies per mL^{-1} per OD_{600}^{-1}). Nevertheless, infected cultures of these
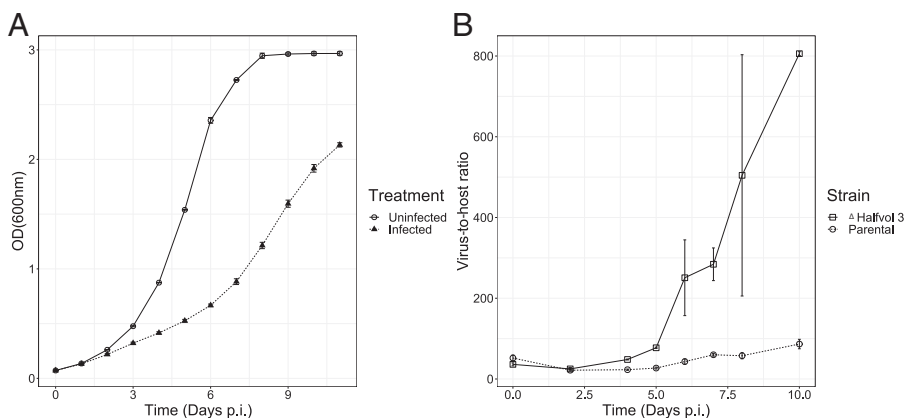
Fig. 6. Virus life cycle in provirus knockout strain. (*A*) Growth curve of uninfected (circle) and infected (black triangles) ΔHalfvol 3 mutant strains cultures. (*B*) VHR calculated by qPCR of virus and host gcn within cells for the parental (open circles) and the mutant strain (open squares). Error bars represent the SD for biological triplicates on both control and treatments.

alternative hosts do not display any significant growth retardation (*SI Appendix*, Fig. S9), which suggests that the virus hijacks host resources and that metabolism is not as pronounced as observed in *H. volcanii*.

Notably, this work represents a report of a promiscuous pleolipovirus, and, while haloarchaeal myoviruses have a very broad host range that crosses the genus level (63, 95), HFPV-1 displays an even broader host range, successfully infecting members of distant lineages at the family level. This versatility of HFPV-1, added to the extreme metabolic remodeling of the host during infection, while possessing a very small genetic repertoire, suggests the existence of global transcriptional regulators on the virus genome and a very conserved receptor on the cell surface across different host lineages. This makes HFPV-1, including its promotors and transcriptional regulators, a great candidate to be developed into a genetic tool, expanding the genetic toolset of model haloarchaea and possibly allowing genetic manipulation of so far inaccessible haloarchaeal strains.

Conclusions

Here we isolated a pleolipovirus infecting the model organism *H. volcanii*. HFPV-1 exhibits a chronic life cycle, being released from host cells without cell lysis and causing only a minor growth retardation despite high viral titers. HFPV-1 does not produce plaques either on *H. volcanii* or on other host organisms, demonstrating that plaque assays are often not suitable to isolate viruses causing a chronic infection and to determine their host range. Furthermore, transcriptional analyses of infected cultures revealed that HFPV-1 infection leads to a radical alteration of the host transcriptional program, with a great proportion of the differentially expressed genes being significantly down-regulated. In particular, we observed that provirus genes in the genome of *H. volcanii* are strongly down-regulated upon HFPV-1 infection, while a knockout strain lacking one of the proviruses experienced a more severe growth retardation than the wild type upon infection. Therefore, we conclude that

the provirus encodes a defense mechanism that is likely based on a repressor gene, and that these virus–virus interactions drive the success and temporal stability of HFPV-1 infection. Furthermore, upon HFPV-1 infection, an inhibition of the host CRISPR-Cas immune system was observed, and none of the other known host defense mechanisms seem to be active for so far unknown reasons.

The establishment of this stable virus–host system in *H. volcanii* opens up the possibility of investigating the influence of a chronic infection on all cellular processes in an archaeal model organism. Additionally, the chronic nature of HFPV-1 infection, together with its wide host range and the high copy number of its genome, makes HFPV-1 a great candidate to be developed as a genetic tool, similar to chronic bacteriophages (6). The small genome could potentially be manipulated within *H. volcanii* and then used for high-yield protein expression in *H. volcanii* or to enable genetic modification of so far inaccessible haloarchaea.

Author affiliations: [a]Max-Planck-Institute for Marine Microbiology, Archaeal Virology, Celsiusstrasse 1, Bremen, 28359 Germany; and [b]The Shmunis School of Biomedicine and Cancer Research, The George S. Wise Faculty of Life Sciences, Tel Aviv University, Tel Aviv 6997801, Israel

1. A. G. Cobián Güemes *et al.*, Viruses as winners in the game of life. *Annu. Rev. Virol.* **3**, 197–214 (2016).
2. S. W. Wilhelm, C. A. Suttle, Viruses and nutrient cycles in the sea aquatic food webs. *Bioscience* **49**, 781–788 (1999).
3. A. E. Zimmerman *et al.*, Metabolic and biogeochemical consequences of viral infection in aquatic ecosystems. *Nat. Rev. Microbiol.* **18**, 21–34 (2019).
4. C. Howard-Varona, K. R. Hargreaves, S. T. Abedon, M. B. Sullivan, Lysogeny in nature: Mechanisms, impact and ecology of temperate phages. *ISME J.* **11**, 1511–1520 (2017).
5. J. Maniloff, J. Das, J. R. Christensen, Viruses of mycoplasmas and spiroplasmas. *Adv. Virus Res.* **21**, 343–380 (1977).
6. S. Mäntynen, E. Laanto, H. M. Oksanen, M. M. Poranen, S. L. Díaz-Muñoz, Black box of phage-bacterium interactions: Exploring alternative phage infection strategies. *Open Biol.* **11**, 210188 (2021).
7. M. K. Pietilä, E. Roine, L. Paulin, N. Kalkkinen, D. H. Bamford, An ssDNA virus infecting archaea: A new lineage of viruses with a membrane envelope. *Mol. Microbiol.* **72**, 307–319 (2009).
8. M. Krupovic; ICTV Report Consortium, ICTV virus taxonomy profile. *J. Gen. Virol.* **99**, 617–618 (2018).
9. S. Roux *et al.*, Cryptic inoviruses revealed as pervasive in bacteria and archaea across Earth's biomes. *Nat. Microbiol.* **4**, 1895–1906 (2019).
10. K. S. Gazi, J. G. Kim, O. Y. Olufowora, U. J. Lee, S. K. Rhee, Prevalence of Nitrosopumilus spindle-shaped viruses in different ecogeographical locations. *Korean J. Microbiol.* **57**, 99–105 (2021).
11. M. K. Pietilä, E. Roine, A. Sencilo, D. H. Bamford, H. M. Oksanen, *Pleolipoviridae*, a newly proposed family comprising archaeal pleomorphic viruses with single-stranded or double-stranded DNA genomes. *Arch. Virol.* **161**, 249–256 (2016).
12. Y. Liu *et al.*, A novel type of polyhedral viruses infecting hyperthermophilic archaea. *J. Virol.* **91**, e00589-17 (2017).
13. R. Hartman *et al.*, Discovery and characterization of thermoproteus spherical piliferous virus 1: A spherical archaeal virus decorated with unusual filaments. *J. Virol.* **94**, e00036-20 (2020).
14. D. Prangishvili, M. Krupovic; ICTV Report Consortium, ICTV virus taxonomy profile. *J. Gen. Virol.* **99**, 1357–1358 (2018).
15. A. Nasir, P. Forterre, K. M. Kim, G. Caetano-Anollés, The distribution and impact of viral lineages in domains of life. *Front. Microbiol.* **5**, 194 (2014).
16. M. K. Pietilä, T. A. Demina, N. S. Atanasova, H. M. Oksanen, D. H. Bamford, Archaeal viruses and bacteriophages: Comparisons and contrasts. *Trends Microbiol.* **22**, 334–344 (2014).
17. A. W. S. Luk, T. J. Williams, S. Erdmann, R. T. Papke, R. Cavicchioli, Viruses of haloarchaea. *Life (Basel)* **4**, 681–715 (2014).
18. A. C. Lindås, E. A. Karlsson, M. T. Lindgren, T. J. G. Ettema, R. Bernander, A unique cell division machinery in the Archaea. *Proc. Natl. Acad. Sci. U.S.A.* **105**, 18942–18946 (2008).
19. J. Liu *et al.*, Archaeal extracellular vesicles are produced in an ESCRT-dependent manner and promote gene transfer and nutrient cycling in extreme environments. *ISME J.* **15**, 2892–2905 (2021).
20. J. Liu *et al.*, Functional assignment of multiple ESCRT-III homologs in cell division and budding in *Sulfolobus islandicus. Mol. Microbiol.* **105**, 540–553 (2017).
21. E. R. J. Quemin *et al.*, Eukaryotic-like virus budding in archaea. *MBio* **7**, 3–7 (2016).
22. D. P. Baquero *et al.*, New virus isolates from Italian hydrothermal environments underscore the biogeographic pattern in archaeal virus communities. *ISME J.* **14**, 1821–1833 (2020).
23. T. A. Demina, H. M. Oksanen, Pleomorphic archaeal viruses: The family *Pleolipoviridae* is expanding by seven new species. *Arch. Virol.* **165**, 2723–2731 (2020).
24. E. V. Koonin, K. S. Makarova, Y. I. Wolf, M. Krupovic, Evolutionary entanglement of mobile genetic elements and host defence systems: Guns for hire. *Nat. Rev. Genet.* **21**, 119–131 (2019).
25. S. Casjens, Prophages and bacterial genomics: What have we learned so far? *Mol. Microbiol.* **49**, 277–300 (2003).
26. S. Roux, S. J. Hallam, T. Woyke, M. B. Sullivan, Viral dark matter and virus–host interactions resolved from publically available microbial genomes. *eLife* **4**, e0849 (2015).
27. S. Benler, E. V. Koonin, Phage lysis-lysogeny switches and programmed cell death: Danse macabre. *BioEssays* **42**, e2000114 (2020).
28. N. Cumby, A. M. Edwards, A. R. Davidson, K. L. Maxwell, The bacteriophage HK97 gp15 moron element encodes a novel superinfection exclusion protein. *J. Bacteriol.* **194**, 5012–5019 (2012).
29. J. Bondy-Denomy, A. R. Davidson, When a virus is not a parasite: The beneficial effects of prophages on bacterial fitness. *J. Microbiol.* **52**, 235–242 (2014).
30. J. Bondy-Denomy *et al.*, Prophages mediate defense against phage infection through diverse mechanisms. *ISME J.* **10**, 2854–2866 (2016).
31. A. A. Vostrov, O. A. Vostrukhina, A. N. Svarchevsky, V. N. Rybchin, Proteins responsible for lysogenic conversion caused by coliphages N15 and φ80 are highly homologous. *J. Bacteriol.* **178**, 1484–1486 (1996).
32. M. J. Lu, U. Henning, Superinfection exclusion by T-even-type coliphages. *Trends Microbiol.* **2**, 137–139 (1994).
33. E. R. J. Quemin *et al.*, First insights into the entry process of hyperthermophilic archaeal viruses. *J. Virol.* **87**, 13379–13385 (2013).
34. S. Medvedeva *et al.*, Virus-borne mini-CRISPR arrays are involved in interviral conflicts. *Nat. Commun.* **10**, 5204 (2019).

35. J. Soppa, From genomes to function: Haloarchaea as model organisms. *Microbiology (Reading)* **152**, 585–590 (2006).

36. D. T. Nieuwlandt, C. J. Daniels, An expression vector for the archaebacterium *Haloferax volcanii*. *J. Bacteriol.* **172**, 7104–7110 (1990).

37. Y. Liao, S. Ithurbide, C. Evenhuis, J. Löwe, I. G. Duggin, Cell division in the archaeon *Haloferax volcanii* relies on two FtsZ proteins with distinct functions in division ring assembly and constriction. *Nat. Microbiol.* **6**, 594–605 (2021).

38. S. D. Nuttall, M. L. Dyall-Smith, HF1 and HF2: Novel bacteriophages of halophilic archaea. *Virology* **197**, 678–684 (1993).

39. D. Ausiannikava et al., Evolution of genome architecture in archaea: Spontaneous generation of a new chromosome in *Haloferax volcanii*. *Mol. Biol. Evol.* **35**, 1855–1868 (2018).

40. M. Dyall-Smith, Halohandbook Version 7.2 (2009). https://haloarchaea.com/halohandbook/.

41. M. Martin, Cutadapt removes adapter sequences from high-throughput sequencing reads kenkyuhi hojokin gan rinsho kenkyu jigyo. *EMBnet. J.* **17**, 10–12 (2013).

42. A. Bankevich et al., SPAdes: A new genome assembly algorithm and its applications to single-cell sequencing. *J. Comput. Biol.* **19**, 455–477 (2012).

43. B. Ushnell, BBMap: A Fast, Accurate, Splice-Aware Aligner. Lawrence Berkeley National Lab.(LBNL), Berkeley, CA (United States), Version 38.06 (2014).

44. D. Hyatt, et al., Prodigal: Prokaryotic gene recognition and translation initiation site identification. *BMC Bioinformatics* **11**, 119 (2010).

45. L. Zimmermann et al., A completely reimplemented MPI bioinformatics toolkit with a new HHpred server at its core. *J. Mol. Biol.* **430**, 2237–2243 (2018).

46. M. Steinegger, M. Mirdita, J. Söding, Protein-level assembly increases protein sequence recovery from metagenomic samples manyfold. *Nat. Methods* **16**, 603–606 (2019).

47. O. Knittelfelder et al., Shotgun lipidomics combined with laser capture microdissection: A tool to analyze histological zones in cryosections of tissues. *Anal. Chem.* **90**, 9868–9878 (2018).

48. A. I. Nesvizhskii, A. Keller, E. Kolker, R. Aebersold, A statistical model for identifying proteins by tandem mass spectrometry. *Anal. Chem.* **75**, 4646–4658 (2003).

49. A. Keller, A. I. Nesvizhskii, E. Kolker, R. Aebersold, Empirical statistical model to estimate the accuracy of peptide identifications made by MS/MS and database search. *Anal. Chem.* **74**, 5383–5392 (2002).

50. R. G. Cutler, J. E. Evans, Synchronization of bacteria by a stationary-phase method. *J. Bacteriol.* **91**, 469–476 (1966).

51. M. I. Love, W. Huber, S. Anders, Moderated estimation of fold change and dispersion for RNA-seq data with DESeq2. *Genome Biol.* **15**, 550 (2014).

52. H. Wickham, *ggplot2: Elegant Graphics for Data Analysis* (Springer-Verlag, New York, 2009).

53. D. Paez-Espino et al., IMG/VR: A database of cultured and uncultured DNA viruses and retroviruses. *Nucleic Acids Res.* **45**, D457–D465 (2017).

54. C. Camacho et al., BLAST+: Architecture and applications. *BMC Bioinformatics* **10**, 421 (2009).

55. S. Roux, J. B. Emerson, E. A. Eloe-Fadrosh, M. B. Sullivan, Benchmarking viromics: An *in silico* evaluation of metagenome-enabled estimates of viral community composition and diversity. *PeerJ* **5**, e3817 (2017).

56. S. W. Cline, W. L. Lam, R. L. Charlebois, L. C. Schalkwyk, W. F. Doolittle, Transformation methods for halophilic archaebacteria. *Can. J. Microbiol.* **35**, 148–152 (1989).

57. T. Allers, H. P. Ngo, M. Mevarech, R. G. Lloyd, Development of additional selectable markers for the halophilic archaeon *Haloferax volcanii* based on the *leuB* and *trpA* genes. *Appl. Environ. Microbiol.* **70**, 943–953 (2004).

58. M. Pohlschroder, S. Schulze, *Haloferax volcanii*. *Trends Microbiol.* **27**, 86–87 (2019).

59. C. Bath, T. Cukalac, K. Porter, M. L. Dyall-Smith, His1 and His2 are distantly related, spindle-shaped haloviruses belonging to the novel virus group, Salterprovirus. *Virology* **350**, 228–239 (2006).

60. J. B. Emerson, B. C. Thomas, K. Andrade, K. B. Heidelberg, J. F. Banfield, New approaches indicate constant viral diversity despite shifts in assemblage structure in an Australian hypersaline lake. *Appl. Environ. Microbiol.* **79**, 6755–6764 (2013).

61. A. Senčilo, L. Paulin, S. Kellner, M. Helm, E. Roine, Related haloarchaeal pleomorphic viruses contain different genome types. *Nucleic Acids Res.* **40**, 5523–5534 (2012).

62. A. L. Hartman et al., The complete genome sequence of *Haloferax volcanii* DS2, a model archaeon. *PLoS One* **5**, e9605 (2010).

63. N. S. Atanasova, E. Roine, A. Oren, D. H. Bamford, H. M. Oksanen, Global network of specific virus-host interactions in hypersaline environments. *Environ. Microbiol.* **14**, 426–440 (2012).

64. M. Krupovic, V. Cvirkaite-Krupovic, J. Iranzo, D. Prangishvili, E. V. Koonin, Viruses of archaea: Structural, functional, environmental and evolutionary genomics. *Virus Res.* **244**, 181–193 (2018).

65. A. Gorlas, C. Geslin, A simple procedure to determine the infectivity and host range of viruses infecting anaerobic and hyperthermophilic microorganisms. *Extremophiles* **17**, 349–355 (2013).

66. S. Breuert, T. Allers, G. Spohn, J. Soppa, Regulated polyploidy in halophilic archaea. *PLoS One* **1**, e92 (2006).

67. C. Howard-Varona et al., Phage-specific metabolic reprogramming of virocells. *ISME J.* **14**, 881–895 (2020).

68. S. Nambi et al., The oxidative stress network of *Mycobacterium tuberculosis* reveals coordination between radical detoxification systems Subhalaxmi. *Cell Host Microbe.* **17**, 829–837 (2015).

69. T. Nyström, F. C. Neidhardt, Expression and role of the universal stress protein, UspA, of *Escherichia coli* during growth arrest. *Mol. Microbiol.* **11**, 537–544 (1994).

70. D. R. Gelsinger, J. DiRuggiero, Transcriptional landscape and regulatory roles of small noncoding RNAs in the oxidative stress response of the haloarchaeon *Haloferax volcanii*. *J. Bacteriol.* **200**, e00779-17 (2018).

71. L. K. Maier, M. Dyall-Smith, A. Marchfelder, The adaptive immune system of *Haloferax volcanii*. *Life (Basel)* **5**, 521–537 (2015).

72. A. J. Molina-Henares, T. Krell, M. E. Guazzaroni, A. Segura, J. L. Ramos, Members of the IclR family of bacterial transcriptional regulators function as activators and/or repressors. *FEMS Microbiol. Rev.* **30**, 157–186 (2005).

73. V. Anantharaman, L. Aravind, Diversification of catalytic activities and ligand interactions in the protein fold shared by the sugar isomerases, eIF2B, DeoR transcription factors, acyl-CoA transferases and methenyltetrahydrofolate synthetase. *J. Mol. Biol.* **356**, 823–842 (2006).

74. E. Okutan et al., Novel insights into gene regulation of the rudivirus SIRV2 infecting *Sulfolobus* cells. *RNA Biol.* **10**, 875–885 (2013).

75. A. C. Ortmann et al., Transcriptome analysis of infection of the archaeon *Sulfolobus solfataricus* with *Sulfolobus* turreted icosahedral virus. *J. Virol.* **82**, 4874–4883 (2008).

76. T. E. F. Quax et al., Massive activation of archaeal defense genes during viral infection. *J. Virol.* **87**, 8419–8428 (2013).

77. S. Fusco et al., Transcriptome analysis of *Sulfolobus solfataricus* infected with two related fuselloviruses reveals novel insights into the regulation of CRISPR-Cas system. *Biochimie* **118**, 322–332 (2015).

78. Y. Ren, Q. She, L. Huang, Transcriptomic analysis of the SSV2 infection of *Sulfolobus solfataricus* with and without the integrative plasmid pSSVi. *Virology* **441**, 126–134 (2013).

79. F. Karlsson, A. C. Malmborg-Hager, A. S. Albrekt, C. A. K. Borrebaeck, Genome-wide comparison of phage M13-infected vs. uninfected *Escherichia coli*. *Can. J.* **51**, 29–35 (2005).

80. P. Nußbaum, M. Gerstner, M. Dingethal, C. Erb, S. V. Albers, The archaeal protein SepF is essential for cell division in *Haloferax volcanii*. *Nat. Commun.* **12**, 3469 (2021).

81. J. Liu et al., Virus-induced cell gigantism and asymmetric cell division in archaea. *Proc. Natl. Acad. Sci.* **118**, e2022578118 (2021).

82. S. V. Albers, K. F. Jarrell, The archaellum: An update on the unique archaeal motility structure. *Trends Microbiol.* **26**, 351–362 (2018).

83. S. Bradde, A. Nourmohammad, S. Goyal, V. Balasubramanian, The size of the immune repertoire of bacteria. *Proc. Natl. Acad. Sci. U.S.A.* **117**, 5144–5151 (2020).

84. M. Li, R. Wang, D. Zhao, H. Xiang, Adaptation of the *Haloarcula hispanica* CRISPR-Cas system to a purified virus strictly requires a priming process. *Nucleic Acids Res.* **42**, 2483–2492 (2014).

85. T. Kuprat, M. Ortjohann, U. Johnsen, P. Schönheit, Glucose metabolism and acetate switch in archaea: Analysis of the enzymes involved in *Haloferax volcanii*. *J. Bacteriol.*, **203** (2021). 10.1128/JB.00690-20.

86. S. L. Díaz-Muñoz, Viral coinfection is shaped by host ecology and virus-virus interactions across diverse microbial taxa and environments. *Virus Evol.* **3**, vex011 (2017).

87. M. Dyall-Smith, F. Pfeiffer, P.-W. Chiang, S.-L. Tang, The novel halovirus Hardycor1, and the presence of active (induced) proviruses in four haloarchaea. *Genes (Basel)* **12**, 149 (2021).

88. M. L. Holmes, F. Pfeifer, M. L. Dyall-Smith, Analysis of the halobacterial plasmid pHK2 minimal replicon. *Gene* **153**, 117–121 (1995).

89. M. Dyall-Smith, F. Pfeifer, A. Witte, D. Oesterhelt, F. Pfeiffer, Complete genome sequence of the model halovirus phiH1 (ΦH1). *Genes (Basel)* **9**, 493 (2018).

90. R. Ken, N. R. Hackett, Halobacterium halobium strains lysogenic for phage phi H contain a protein resembling coliphage repressors. *J. Bacteriol.* **173**, 955–960 (1991).

91. S. Erdmann, S. Le Moine Bauer, R. A. Garrett, Inter-viral conflicts that exploit host CRISPR immune systems of *Sulfolobus*. *Mol. Microbiol.* **91**, 900–917 (2014).

92. A. Luque, C. B. Silveira, Quantification of lysogeny caused by phage coinfections in microbial communities from biophysical principles. *mSystems* **5**, e00353-20 (2020).

93. C. M. Mizuno et al., Novel haloarchaeal viruses from Lake Retba infecting *Haloferax* and *Halorubrum* species. *Environ. Microbiol.* **21**, 2129–2147 (2019).

94. E. A. Becker et al., Phylogenetically driven sequencing of extremely halophilic archaea reveals strategies for static and dynamic osmo-response. *PLoS Genet.* **10**, e1004784 (2014).

95. N. S. Atanasova, T. A. Demina, A. Buivydas, D. H. Bamford, H. M. Oksanen, Archaeal viruses multiply: Temporal screening in a solar saltern. *Viruses* **7**, 1902–1926 (2015).

96. T. Alarcon-Schumacher, A. Naor, U. Gophna, S. Erdmann. Haloferax pleomorphic virus 1 (HFPV-1). National Center for Biotechnology Information GenBank database. https://www.ncbi.nlm.nih.gov/nuccore/OM621814. Deposited 8 February 2022.

97. T. Alarcon-Schumacher, A. Naor, U. Gophna, S. Erdmann. Haloferax volcanii infected with HFPV-1 virus. European Nucleotide Archive. https://www.ebi.ac.uk/ena/browser/view/PRJEB50750. Deposited 8 February 2022.